Multi-band MEG signatures of BOLD connectivity reorganization during visuospatial attention

Chiara Favaretto [a,h,*], Sara Spadone [b], Carlo Sestieri [b], Viviana Betti [c,d], Angelo Cenedese [e], Stefania Della Penna [b,1], Maurizio Corbetta [a,f,g,h,1,*]

[a] Department of Neuroscience and Padova Neuroscience Center, University of Padova, 35128 Padova, Italy
[b] Department of Neuroscience, Imaging and Clinical Sciences – and ITAB, Institute for Advanced Biomedical Technologies, G. d'Annunzio University of Chieti-Pescara, 66100 Chieti, Italy
[c] Department of Psychology, Sapienza University of Rome, 00185 Rome, Italy
[d] IRCCS Fondazione Santa Lucia, 00179 Rome, Italy
[e] Department of Information Engineering, University of Padova, 35131 Padova, Italy
[f] Department of Neurology, Radiology, Neuroscience, and Biomedical Engineering Washington University Saint Louis, MO 63110, USA
[g] Venetian Institute of Molecular Medicine, VIMM, 35128 Padova, Italy
[h] Padova Neuroscience Center, PNC, 35131 Padova, Italy

ARTICLE INFO

ABSTRACT

The functional architecture of the resting brain, as measured with the blood oxygenation level-dependent functional connectivity (BOLD-FC), is slightly modified during task performance. In previous work, we reported behaviorally relevant BOLD-FC modulations between visual and dorsal attention regions when subjects performed a visuospatial attention task as compared to central fixation (Spadone et al., 2015).

Here we use magnetoencephalography (MEG) in the same group of subjects to identify the electrophysiological correlates of the BOLD-FC modulation found in our previous work. While BOLD-FC topography, separately at rest and during visual attention, corresponded to neuromagnetic Band-Limited Power (BLP) correlation in the alpha and beta bands (8–30 Hz), BOLD-FC modulations evoked by performing the visual attention task (Spadone et al. 2015) did not match any specific oscillatory band BLP modulation. Conversely, following the application of an orthogonal spatial decomposition that identifies common inter-subject co-variations, we found that attention–rest BOLD-FC modulations were recapitulated by multi-spectral BLP-FC components. Notably, individual variability of alpha connectivity between Frontal Eye Fields and visual occipital regions, jointly with decreased interaction in the Visual network, correlated with visual discrimination accuracy. In summary, task-rest BOLD connectivity modulations match multi-spectral MEG BLP connectivity.

1. Introduction

In the resting state, several studies have shown that the topography of fMRI networks is recapitulated by the topography of slow (<0.1 Hz) coherent fluctuations of band-limited power (BLP) (de Pasquale et al., 2010; de Pasquale et al., 2012) especially in the alpha and beta frequency bands (Brookes et al., 2011b, 2011a; de Pasquale et al., 2010; de Pasquale et al., 2012; Hipp et al., 2012; Liu et al., 2010) or SNR-corrected multi-band patterns (Hipp and Siegel, 2015). In contrast, the literature on the comparison of BOLD vs. MEG connectivity during task conditions is scant. This is possibly due to the high similarity of the task and rest global interaction patterns, as observed, separately, in fMRI (Cole et al., 2014; Smith et al., 2009; Spadone et al., 2015; Tavor et al., 2016) and MEG (Betti et al., 2018, 2013).

The few BOLD-MEG connectivity comparison studies showed similar functional connectivity topography for slow oscillations (<30 Hz, see (Betti et al., 2013; Liljeström et al., 2015)). Betti et al. (Betti et al., 2013) compared fMRI and BLP connectivity during visual fixation (rest)

and the observation of a movie (task). While the overall topography was maintained, the task-induced BOLD connectivity decreases in multiple networks, which corresponded to a decrease of alpha and beta BLP connectivity (<30 Hz). In contrast, BLP connectivity in other frequencies (theta, beta, and gamma) increased, corresponding to both increases or decreases of BOLD connectivity.

Liljeström et al. (Liljeström et al., 2015) compared fMRI and MEG networks when subjects named either actions or objects presented on a screen vs. when they simply saw the same stimuli. As Betti et al., they found the greatest similarity in MEG and fMRI derived networks for neural frequencies below 30 Hz. However, BOLD network task vs rest modulations could not be attributed to a single frequency band. Instead, the entire spectral profile was the best descriptor of the correspondence between MEG and fMRI networks.

In this study, we revisit the question of rest-task fMRI vs. MEG connectivity modulations using a well-controlled visuospatial attention task. This experiment introduces several innovations as compared to previous studies. First, the task is highly controlled psychophysically, as compared to previous studies that used naturalistic stimulation with no behavioral control (Betti et al., 2013) or covert responses (Liljeström et al., 2015). This attention paradigm has been employed in multiple experiments (Capotosto et al., 2015, 2013; Shulman et al., 2010, 2009; Spadone et al., 2015). Subjects either maintain visual fixation (rest) or perform a visuospatial attention task in which the focus of attention is covertly directed to a left or right stimulus stream based on iso-luminant color cues embedded in the visual stream. The detection of targets, by key press, occurs either on the same or opposite side of attention. The relative advantage in accuracy and reaction times for attended vs. unattended targets is a probe of the allocation of visuospatial attention.

Secondly, the functional anatomy is known as compared to previous work in which the regions of interest were predefined based on prior parcellations (Betti et al., 2013) or source localized MEG signals on the same task (Liljeström et al., 2015). Based on fMRI experiments ran on the same subjects (Spadone et al. 2015), we knew that a relatively small set of cortical regions were modulated by attention. These included occipital visual regions (VIS), sensitive to the location (left, right) of attention, and regions of the so-called dorsal attention network (DAN), sensitive to shifts of attention. Therefore, we used source localized MEG signals from this specific set of functional regions.

Thirdly, we have a hypothesis on the direction of BOLD functional connectivity (BOLD-FC) modulations induced when going from visual fixation (rest) to visuospatial attention (task) (Spadone et al. 2015). BOLD-FC connectivity nicely segregates DAN and VIS regions both during fixation and task, but the two networks increase their correlation during the task in parallel with a relative decrement of connectivity within the VIS network.

The aims of the study were twofold: to compare the patterns of task-induced modulation of fMRI and MEG connectivity, specifically within- vs. between-network interactions; and, to examine whether the correspondence between BOLD and BLP connectivity topography and relative task-modulation, is better accounted for by single vs. multi-band spectral patterns.

2. Materials and Methods

2.1. Subjects

Twenty healthy subjects (age range = 19–28 y old; 14 females), right-handed (Edinburgh Inventory), participated in both the fMRI and MEG scans. The original sample size of (Spadone et al., 2015) consisted of 21 subjects, but 1 subject was excluded due to the incompatibility of the head size with the MEG helmet. The subjects, with no previous psychiatric or neurological history, provided their informed written consent according to the Code of Ethics of the World Medical Association and the Institutional Review Board and Ethics Committee at the University of Chieti. This group of subjects was enrolled through a preliminary behavioral session, during which they performed a continuous visuospatial attention task similar to the task of the neuroimaging scans (see subsection Stimulation Paradigms) to evaluate performance and eye position with an IR eye-tracking system (Iscan etl-400; RK-826 PCI) (Spadone et al., 2015).

2.2. Stimulation Paradigms

Pseudorandom sequences of continuous reorienting/maintenance stimuli (Capotosto et al., 2015, 2013), all generated using the MAT-LAB Psychtoolbox-3 (Brainard, 1997; Kleiner et al., 2007; Pelli, 1997), were delivered to the subjects. Stimuli consisted of two continuous drifting Gabor patches, 3° diameter, 2 cycle/° spatial frequency, 0.7°/s drift rate. The two patches were presented onto a screen, over a light grey background, at both sides of a central fixation cross at an eccentricity of 5.5°. During the fMRI study, stimuli were projected (using an EIKI LC XG-250L Projector System) on a screen situated behind the subject's head and viewed through a mirror located above the subject's head. For the MEG study, we used an LCD projector (NEC MT830G+) placed outside the shielded room, projecting images on a pair of 45° mirrors and a translucent screen. For both projectors: the horizontal Sync was automatically set in the range 15–100 kHz; the vertical Sync in the range 50–100 Hz.

Participants were instructed to maintain central fixation while covertly attending one of the two gratings to detect briefly presented targets. The side to be attended was indicated by a peripheral cue consisting of a 300 ms isoluminant change in the color (pink and cyan) simultaneously applied to the two patches. Only one color, indicated at the beginning of each block and counterbalanced across blocks, was relevant for cueing. The cue could appear in the same location as the previous trial (stay cue) or the opposite location (shift cue), indicating that the attention had to be shifted. The targets consisted of brief (150 ms) changes of the patch orientation in either clockwise or anti-clockwise direction, which should be signaled by the subjects by pressing the right/left button with their right middle or index finger on a response pad. The cue correctly predicted the location of the target with 80% probability (valid trials), whereas the target appeared at the uncued location (invalid trials) in 20% of the trials. Cues appeared at random intervals between 4 and 6 s, in the MEG session, and every 2, 3, 4 repetition times (TR) within a temporal window of +/-400 ms centered on the TR, in the fMRI session. After each cue, either zero, one, or two targets could be presented. Cues did not predict when the target would appear, but they were linked by three temporal constraints: (i) targets could not occur earlier than 1 s after a cue (ii) cues could not occur earlier than 2 s after a target (iii) targets occurred, on average, every 11 s in the MEG session and every 9 s in fMRI (see Fig. 1A for an example of the display sequence). Finally, we generated two pseudorandom stimulus sequences of ~16 min for the MEG session, each consisting of three blocks of attention task lasting 300 s and interleaved by 15 s periods of fixation, used to minimize fatigue and drop of attention. For the fMRI session, we generated 12 pseudorandom sequences, each lasting 210 s.

2.3. fMRI recordings

The fMRI hardware specifications and acquisition protocols were already extensively described in (Spadone et al., 2015). Briefly, BOLD contrast was obtained from T2*-weighted images collected on a Philips Achieva 3T Scanner using a gradient echo-planar imaging sequence [TR = 1.869 ms; Time of Echo (TE) = 25 ms; 39 slices acquired in ascending interleaved order; voxel size = $3.59 \times 3.59 \times 3.59$ mm^3; 64×64 matrix; and flip angle = 80°]. Structural images, to be used also for MEG processing, were collected using a sagittal M-PRAGE T1-weighted sequence (TR = 8.14 ms; TE = 3.7 ms; flip angle = 8°; voxel size = $1 \times 1 \times 1$ mm^3).
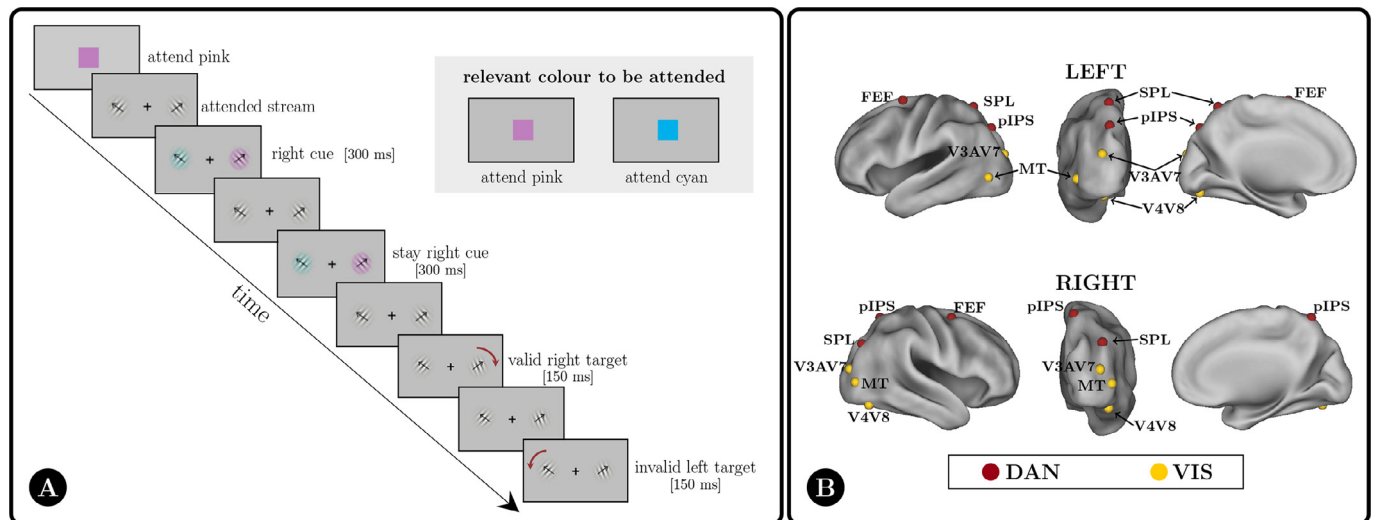
Fig. 1. Paradigm and involved ROIs. A) Example of the stimulus stream in the visuospatial attention task. B) Representation of the ROIs involved during the performed task. These ROIs were selected in (Spadone et al., 2015), on the same subjects scanned by MEG, based on their fMRI response profile during the attention task. Different networks are color-coded (red: Dorsal Attention Network (DAN); yellow: Visual Network (VIS)).

The fMRI session included 3 resting-state runs (each lasting 5 min) and 12 runs of task. An MRI-compatible IR eye-tracking system (Iscan etl-400; RK-826 PCI) was used to control eye movements. Subjects' responses were collected through a LUMINA LU400 Response Pad (Cedrus Corporation).

2.4. MEG Recordings

MEG scans were obtained through a custom-made whole head system developed, installed, and operating at the University of Chieti since about 2000 (Della Penna et al., 2000; Pizzella et al., 2001). The system was implemented in collaboration with the current ATB Biomag UG. The MEG system consists of 153 dc SQUID magnetometers placed on a helmet-shaped surface covering the whole scalp and spaced about 3.2 cm. The sensors are housed inside a low-noise dewar with a helmet-shaped bottom, at a distance of 1.8 cm from room temperature. MEG signals, together with two ECG and two EOG channels to be used for offline artifact rejection and for monitoring horizontal eye movements, were band-passed at 0.1–250 Hz and sampled at 1025 Hz. Stimuli were projected onto a screen situated inside the magnetically shielded room. Subjects responded using a LUMINA LU400 Response Pad (Cedrus Corporation). A MEG session consisted of 3 runs of fixation lasting 5 min each, followed by 2 runs of the visuospatial attention task. After each run, the subject's head position relative to the MEG sensors was estimated from the field produced by five coils placed on the scalp, whose positions were digitized together with 5 anatomical landmarks.

2.5. Preprocessing and FC Evaluation

2.5.1. fMRI Data Analysis

The preprocessing procedures, the ROI identification, and the FC evaluation are extensively described in (Spadone et al., 2015) and in *Supplementary Material S1.1*. Briefly, in our previous study, we aimed to identify regions showing activity modulation due to the cue type (shift, stay) or the cue location (left, right). Following standard preprocessing, we employed a generalized linear model (GLM) that made no a priori assumption of the hemodynamic response shape, by generating separate Δ-function regressors for each of seven MR frames starting at the onset of cues and targets. The GLM used 12 types of regressors including first cues (left, right), standard cues (shift left, shift right, stay left, and stay right), targets (valid left, valid right, invalid left, and invalid right), and additional regressors coding for baseline and linear trend in each scan.

Significant ROIs were identified through a voxel-wise ANOVA with cue type (stay and shift), cue location (left and right), and time as factors on the time courses of the evoked responses to cue stimuli. The voxel-wise ANOVAs were corrected for non-independence of time points by adjusting the degrees of freedom and corrected for multiple comparisons using a joint z-score/cluster size threshold (Forman et al., 1995) corresponding to z = 3.0 and a cluster size of 13 face contiguous voxels. A peak-search algorithm was applied to the cue type by time, and cue location by time statistical maps resulting in the selection of 6 ROIs belonging to the Dorsal Attention Network (DAN – the superior parietal lobule (SPL), the dorsal aspect of the human frontal eye fields (dFEF), and the posterior intraparietal sulcus (pIPS), all bilateral), showing stronger shift-related than stay-related activity, and 6 ROIs of the Visual Network (VIS – the ventral V4-V8, the dorsal V3a-V7 in the occipital cortex and the lateral middle temporal (MT) visual area, bilaterally), showing spatially selective effects (contralateral stronger than ipsilateral activity). These ROIs are shown on an MNI brain surface in Fig. 1B. Following removal of the BOLD response evoked by the cues and targets, and of the signal averaged over the whole brain, a low pass filter with a cutoff at 0.167 Hz was applied. Static connectivity matrices at task and during fixation were estimated through the z-Fisher transform of the pairwise Pearson's correlation coefficients averaged across runs (as computed in (Spadone et al., 2015)).

2.5.2. MEG Data Analysis

Following the data quality check of the channel-level MEG data (Larson-prior et al., 2013), 2 subjects were excluded due to the presence of abnormal artifacts. For sake of data comparison, the same 2 participants were excluded from the fMRI analysis, as well. MEG data were analyzed through the following steps (see Figure 2A): (i) a pipeline based on Independent Component Analysis (ICA) followed by an automatic classification procedure aimed to identify the brain and artifactual Independent Components (ICs) (de Pasquale et al., 2012; Mantini et al., 2011; Sebastiani et al., 2014; Spadone et al., 2012) was applied to the channel data (see *Supplementary Material S1.2.1* for more details). Then, (ii) the sensor maps of the brain IC were projected in the source space using a weighted minimum-norm least square (wMNLS) estimator implemented in Curry 6.0 (Neuroscan), using a realistic model of the source space and volume conductor obtained from the subject's anatomical image and sampled by a Cartesian 3D grid with 4 mm voxel side (see *Supplementary Material S1.2.2* for more details). The individual source maps were then transformed into MNI152 space to enable subsequent spatial
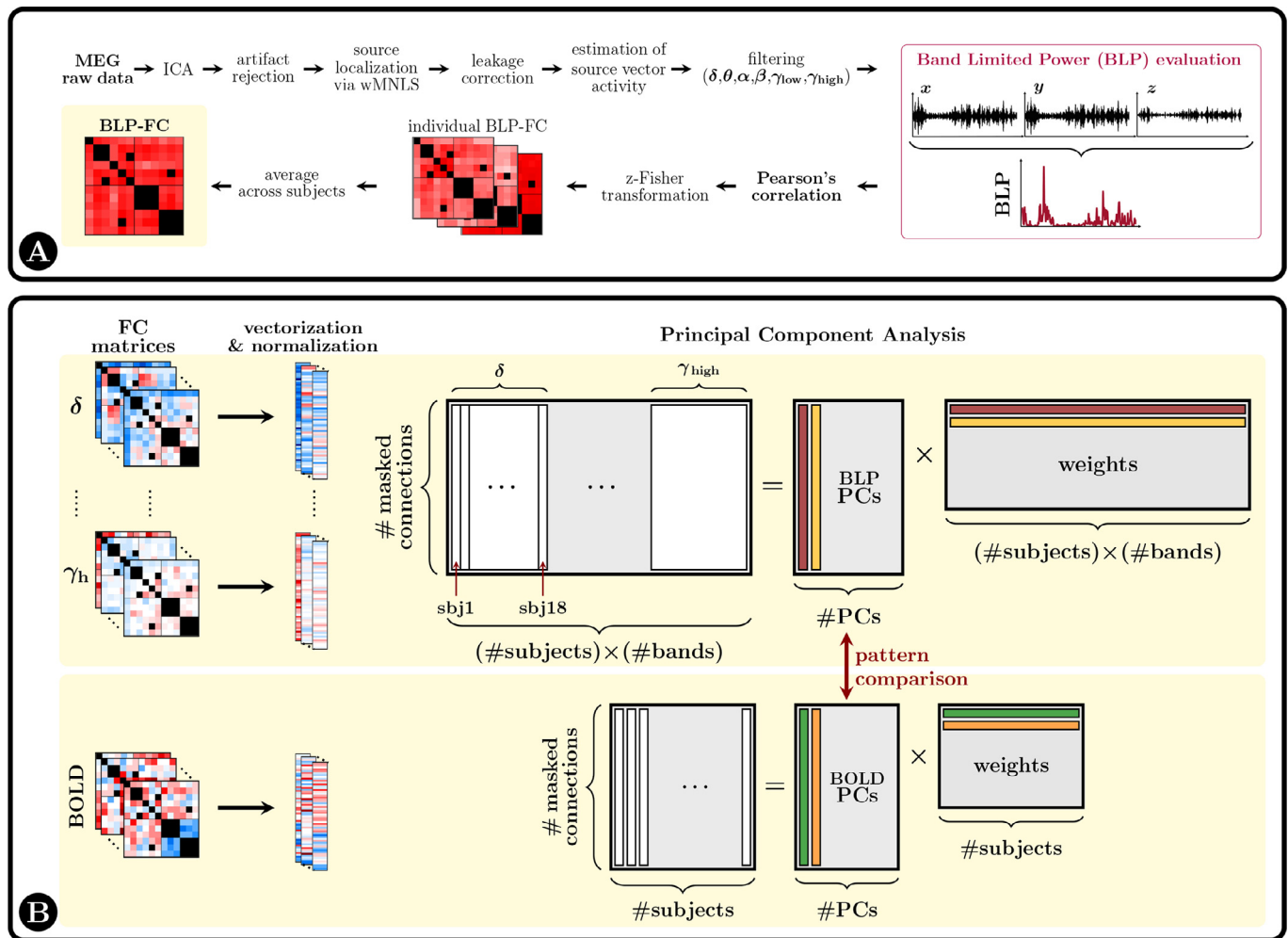
Fig. 2. Methods. A) Processing strategy steps to obtain the BLP-FC matrices from the MEG raw data. After preprocessing, aimed at removing artifacts and projecting channel-level signals into the source space, MEG source activity is filtered in six frequency bands to estimate the BLP signal. Individual BLP-FC is estimated through Pearson's correlation coefficient (z-Fisher transformed). Finally, the individual matrices are averaged across subjects to generate the group BLP-FC for each frequency band. B) Flowchart of the multi-band comparison between the BLP- and BOLD-FC matrices. Individual, vectorized FC matrices (rest, task or task–rest) are concatenated (across frequencies and subjects together, in case of BLP-FC) and used as input for the PCA, which decomposes the original matrices into the product of the PCs and the weights of each PC across subjects (and bands, in case of BLP). Finally, the BLP- and BOLD-derived PCs are compared using Mantel's Tests.

averaging across subjects. We decided to use a volume grid because the BOLD-FC data from Spadone et al., 2015 were obtained from a 3D grid into the 711-2C atlas, which was then co-registered to MNI, and we wanted to use the same type of source volume to facilitate the comparison among FC matrices (e.g. we did not want to introduce any confound due to handling seeds into different source spaces grid and cortical mantle). Moreover, coregistration of the individual source space to the MNI space is more straightforward, facilitating group average. At this point, (iii) for each voxel corresponding to the peak activity of the 12 ROIs identified from fMRI (namely seed from now on) we corrected the leakage effects on the source space maps according to the Geometrical Correction Scheme (Wens et al., 2015) applied to the linear inverse operator $W = \sum_{ic} A_{ic} u_{ic}$ as in (Betti et al., 2018; Della Penna et al., 2019), where u_{ic} is the row of the unmixing matrix associated with the source map A_{ic} for a generic independent component IC (see *Supplementary Material S1.2.3* for more details). For each seed, (iv) the voxel vector activities of the other seeds were estimated as a linear combination of the IC time courses, each weighted by the related leakage-corrected source map value. For each seed and vector signal direction the contribution of the evoked signal was adaptively removed from each cue and target as in (Della Penna et al., 2004) (see *Supplementary Material S1.2.4* for more details). Then, (v) all the leakage-corrected signals together

with the seed itself were filtered in delta (δ) [1–4] Hz, theta (θ) [4–8] Hz, alpha (α) [8–14] Hz, beta (β) [14–30] Hz, low-gamma (γ_l) [30–50] Hz and high-gamma (γ_h) [50–120] Hz bands. (vi) For each seed, a set of MEG Band Limited Power (BLP) time series at voxel were estimated by averaging instantaneous source-space power over sliding windows of duration = 150 ms and step of 20 ms. Finally, (vi) the individual, leakage-corrected BLP Functional Connectivity maps were obtained using pair-wise Pearson's correlation coefficient, followed by z-Fisher transformation. Connectivity values between regions closer than 3.5 cm were masked to account for possible miscorrection effects due to seed mislocalization (Wens et al., 2015).

Eventually, the group FC at each frequency band was obtained by averaging individual FC matrices across subjects.

2.6. Comparison between BOLD- and Single-Band BLP-FC Matrices

The first step was to compare the BOLD and BLP-FC matrices in the single rest or task conditions. We first tested RSN segregation for each modality using a t-test comparing within vs. between average correlation, averaging the FC values over each sub-matrix (DAN, VIS, and DAN-VIS). For BOLD FC, this test was already carried out in (Spadone et al., 2015), thus we refer to the methods and results reported in that paper.

Then we compared the patterns obtained by the two modalities through a regression analysis on all the pairwise correlation values for each subject, where the BOLD- and single-band BLP-FC data were considered as the independent, and the dependent variables, respectively and we tested the significance of the regression coefficient vs. 0 through a t-test over subjects.

Secondly, we searched for BLP correlates of task-induced BOLD-FC modulations at the level of the whole matrix and sub-matrices, based on the correlation strength and correlation pattern. (i) The first type of comparison considered the sign polarity of the task vs. rest correlation differences. Given that (Spadone et al., 2015) reported in task-minus-rest FC no FC change between DAN regions, an FC decrease between VIS regions, and an FC increase between VIS and DAN regions, respectively, we looked for their spectral signatures. Hence for both modalities (and separately for each frequency band), the mean pairwise connectivity over task–rest matrices or submatrices was compared vs. 0 through a 2-tailed t-test over subjects ($p < 0.05$, Bonferroni corrected across 6 bands). The submatrices included only pairwise correlations between regions that belonged respectively to the VIS only, DAN only, or VIS-DAN. (ii) The second analysis looked for the similarity of task–rest correlation patterns on the whole matrix and sub-matrices for each band. As in the single condition, we first compared the whole matrices applying a linear regression analysis over the node pairs for each subject. The regression coefficients were tested vs. 0 through a t-test, Bonferroni corrected for 6 (the number of frequency) multiple comparisons. The same strategy was applied to sub-matrices, together with additional analyses described in the *Supplementary Material (S1.3 and S2.1)*.

2.7. Comparison Between BOLD- and Multi-Band BLP-FC Principal Components

In addition to the standard analyses described in the previous subsection, we investigated whether the FC matrices could be decomposed into connectivity patterns (components) that were common across subjects. This strategy was motivated by the hypothesis that while in single conditions the connectivity patterns were dominated by the contribution of a larger within- than between-network connectivity as already revealed in (Spadone et al., 2015), in the task vs. rest difference a larger inter-subject variability might emerge. In this case, separation techniques are useful for the following reasons: (i) to extract information from the data; (ii) to select common (across subjects) spatial patterns of task-induced connectivity changes without a-priori assumptions; (iii) to reduce the number of variables to be compared. Thus, we applied a spatial separation, through (not-centered) Principal Components Analysis (PCA), to BOLD- and multivariate BLP-FC, as shown schematically in Fig. 2B, for single condition (rest and task), separately, and the difference task vs. rest. We also applied PCA to single band BLP-FC, and a description of methods and results are reported in the *Supplementary Material (S1.4 and S2.3)*. First, for each condition, individual BOLD-FC masked matrices were vectorized (unrolling the upper triangular FC matrix) and normalized to the maximum absolute FC value, to obtain a BOLD-FC vector of dimension 57 for each subject (this dimension accounts for the exclusion of the same pairs which were masked in the BLP FC matrix). These individual vectors were arranged in a matrix of FCs, with dimension 57×18, where 18 was the number of subjects. The spatial PCA decomposed this matrix into the product of the BOLD-PCs (matrix dimensions $57 \times N_{PC\text{-}BOLD}$) and the related weights of each BOLD-PC across subjects (matrix dimensions $N_{PC\text{-}BOLD} \times 18$).

Similarly, for each frequency band separately, the vectorized, masked, and normalized BLP-FC was organized into an input matrix with dimension 57×18. Then, all frequency bands were arranged into a single input matrix with dimension $57 \times (18 \times 6)$, where the band-specific vectorized FC matrices were concatenated across subjects for each band. Note that for BLP-FC, the maximum FC value has been evaluated among all the frequency bands, to preserve the inter-bands relationships. The spatial PCA applied to this matrix produced a BLP-PCs

matrix (matrix dimensions $57 \times N_{PC\text{-}BLP}$) and a weight matrix across frequency bands and subjects (matrix dimensions $N_{PC\text{-}BLP} \times (18 \times 6)$). For each modality, the number of PCs to be considered for the similarity analysis was identified applying an automatic selection method, defined as the *elbow method*, which consists in the identification of the elbow point along the scree plot of the explained variance of each component (Cattell, 1966; Lattin et al., 2003). Variance values below the elbow are considered too small, and the related components are discarded.

BOLD-PCs and multi-band BLP-PCs were compared through Mantel's test (Mantel and Haenszel, 1959), which is used to calculate the correlations between corresponding positions of two similarity symmetric matrices derived from multivariate data. Specifically, the test uses the unfolded upper triangular part of each matrix and evaluates the correlation coefficient between these vectors. Mantel statistics were tested for significance by 15,000 permutations, during each of which the rows and columns of either one of the two matrices were permuted and the Mantel statistic was recomputed to determine the expected distribution of the statistic under the null hypothesis. Finally, the value obtained from the observed data was compared to the null distribution, to assess the statistical significance.

Before comparing the obtained PCs across methods, we run a procedure to identify the PC polarity, which is undetermined in PCA. Specifically, each BOLD-PC polarity was selected to be positively correlated with the group-level BOLD FC matrix. The polarity of the BLP-PCs was instead set to produce, for the BLP-PC, a positive maximum correlation with the BOLD-PCs.

The robustness of the PC test was analyzed through a leave-one-out test described in *Supplementary Materials (S1.5 and S2.4)*.

2.8. Task–Rest Multi-Band BLP-FC Components and Target Discrimination Accuracy

To explore the relationship between task-induced connectivity BLP modulation and the behavioral performance, for each task–rest multi-band BLP-PC, we evaluated the significance of the associated oscillatory bands. First, we evaluated the subject-wise relative participation weight (in absolute value) of each frequency band, normalized to the individual weight sum. In this manner, for each subject, and each BLP-PC we obtained a vector of 6 components, indicating the percentage contribution (in absolute value) of each frequency band. The individual target discrimination accuracy was binarized in high and low performance levels concerning the mean accuracy across subjects. For each task–rest BLP-PC, we tested possible differences of the relative participation weights across bands using a two-way multivariate ANOVA across subjects, with bands as the within-subjects factor and binary performance as the across-subjects factor.

All BOLD and BLP averaged functional connectivity matrices, as well as BOLD and BLP-PCs (rest, task, and task–rest) with related participation weights, are available in "Mendeley Data" (https://data.mendeley.com/).

3. Results

3.1. Single-band Comparison between fMRI and MEG Connectivity Matrices

The group average BOLD- and BLP-FC matrices at rest and task, and their difference (task–rest) are shown in Fig. 3. Each row represents an ROI of the DAN, and then the VIS network and the color scale represents the pairwise correlation (z-Fisher transformed). Blackened cells indicate region pairs closer than 3.5 cm and masked for further analyses based on the leakage correction algorithm (Wens et al., 2015) (see Materials and Methods - *MEG data analysis* and *Supplementary Material S1.2.3*).

First, let's focus on separate rest and task matrices. BOLD-FC matrices include both positive and negative weights (i.e., positive and negative correlation) while BLP-matrices contain only positive weights. We think
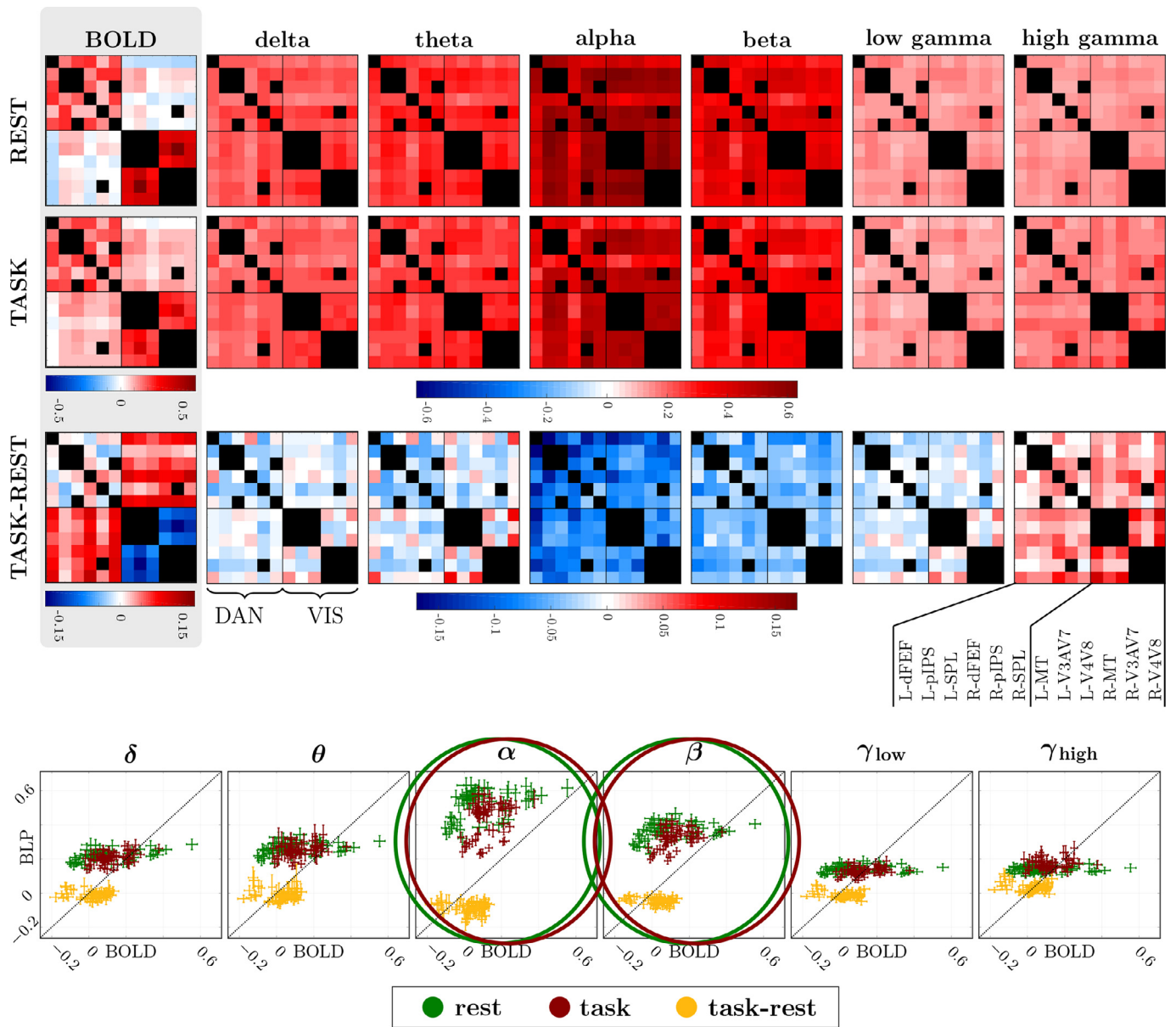
Fig. 3. Functional Connectivity values. Top) Averaged BOLD-FC matrices (gray-shaded area) and averaged BLP-FC matrices for each frequency band (from delta to high gamma) for rest, task, and task–rest difference. Black areas indicate functional connections that were masked out from the MEG data analysis due to the spatial closeness of the corresponding ROI pair. The same mask is applied to BOLD-FC for comparison. While the average was used to define these group connectivity matrices, the following analyses are based on individual data. Bottom) Scatter plot of the BLP functional connections (y-axis), separate for each band, versus the BOLD functional connections (x-axis) for rest (green), task (red), and task–rest difference (yellow). Each cross stands for a single cell of the FC matrix, centered at the average across subjects, and with the arms' length equal to the standard error across subjects. A black dotted line indicates the bisector. Green and red circles indicate significant regressions in rest and task, respectively. In these plots, it not possible to find any clear evidence of a linear relationship between BLP-FC and BOLD-FC values for task–rest matrices.

this is due to the whole-brain signal regression, a step taken in the fMRI preprocessing that centers the correlation values around 0. This step is not easily implemented in the MEG preprocessing (see Discussion), but it will be essentially dealt with in the PCA analysis described in the next section. Secondly, DAN and VIS networks are clearly segregated in BOLD-FC matrices, and the correlation between regions of the DAN and the VIS network significantly increases during the task ($p < 10^{-4}$; t-test), as shown in (Spadone et al., 2015), where all the statistical analyses were reported. In the BLP-FC matrices, we also observe network segregation. In fact, within-network BLP correlation is stronger than between-network BLP correlation at rest and task in several bands (rest: delta, theta, alpha, beta, low gamma, all $p < 0.05$; task: delta, theta, alpha, beta, low-gamma, high-gamma, all $p < 0.05$; all ps Bonferroni

corrected), as assessed through t-tests. The increase in DAN-VIS correlation is observed only for high-gamma connectivity, but the p-value was not significant anymore after Bonferroni correction ($p = 0.011$, before correction).

To analyze the relationship between FC patterns at rest and during task, at the group level, we arranged the FC values into scatter plots and estimated the regression coefficients. These plots are shown at the bottom of Fig. 3, in which we display the mean and standard error (across subjects) of the BOLD (x-axis) and BLP (y-axis) FC values of each node pair, for each band and condition (i.e., rest in green, task in red, and task–rest in yellow). Focusing on the task and rest conditions, we found significant regression coefficients only in the alpha and beta bands in both task ($b_\alpha = 0.17$, p-alpha = 0.038; $b_\beta = 0.14$, p-beta = 0.0012, all
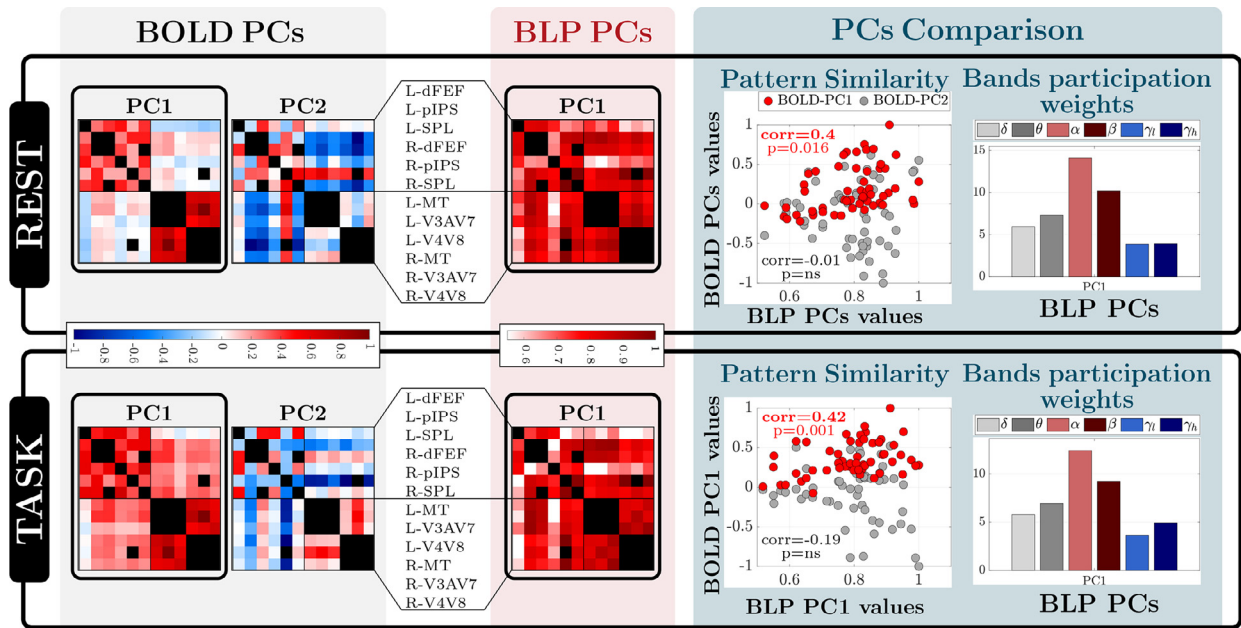
Fig. 4. Comparison between multi-band BLP- and BOLD- Principal Components at rest (Top) and task (Bottom). Left) BOLD Principal Components (PC1 and PC2). Middle) Multi-band BLP-PCs. Right) Left column: scatter plot of BOLD-PC1 (red dots) and BOLD-PC2 (gray dots) vs. BLP-PC1 pairwise regional connectivity values (*p*-values assessed through Mantel's test, Bonferroni corrected). Note the significant correlation between BOLD-PC1 and BLP-PC1. Right column: participation weights of each frequency band to the BLP-PCs, evaluated as the sum of the absolute weight values across subjects.

Bonferroni corrected) and rest ($b_\alpha = 0.17$, p-alpha = 0.0024; $b_\beta = 0.08$, p-beta = 0.025, all Bonferroni corrected). Therefore, these results show a significant spatial similarity of group average BOLD-FC and BLP-FC topography at rest and during tasks, even though task correlation values are lower.

Next, let's consider the difference BOLD-FC matrix (task–rest). A significant decrease of within-VIS correlation was paralleled by a correlation increase between VIS and DAN regions, as already reported in (Spadone et al. 2015)). The picture for BLP-FC was more complex. There was an overall decrease of connectivity in two bands, assessed through t-test across subjects of average coupling strength vs. 0: alpha (t-val = -3.90, p-val = 0.0016) and beta bands (t-val = -4.25, p-val = 0.0005). There is also increased correlation in the high-gamma band (t-val = 2.5536, p-val = 0.02). In delta, theta, and low-gamma bands, both increases and decreases were found depending on the specific pair of regions.

However, at the level of a single band, none of these spatial patterns was linearly related to the pattern of task-evoked FC modulation measured in fMRI. This is confirmed in the scatter plots of Fig. 3 bottom (yellow crosses), where no regression coefficient was significantly different from 0 ($b_\delta = -0.04$; $b_\theta = -0.02$; $b_\alpha = 0.001$; $b_\beta = 0.02$; $b_{\gamma_l} = -0.04$; $b_{\gamma_h} = -0.03$; all ps = n.s.). However, qualitatively, across bands, some of the salient BOLD-FC modulations are evident. For instance, BOLD-FC decrements in the VIS network correspond to both alpha-beta decrements and theta-gamma BLP-FC increases. Similarly, DAN-VIS BOLD-FC increments correspond to both alpha-beta decreases, and high gamma BLP-FC increases. This suggests that multi-band modulations may be important to describe task-dependent changes in connectivity.

3.2. Comparison between BOLD- and Multi-Band BLP- FC Components

Given the lack of a clear BOLD-BLP FC correspondence at the level of group-averaged data and single BLP bands and the presence of a large common signal in the MEG BLP matrices, we performed an analysis to seek similar spatial component patterns across subjects and modalities. Therefore, we ran a separate PCA on BOLD and single-band BLP correlation matrices and compared the obtained principal components (PCs)

across modalities. We applied this data-driven spatial pattern separation both in single conditions (rest and task) separately, and in task–rest data. For both fMRI and MEG data and every condition, we selected the components to be retained for the analysis through the automatic *elbow method*, to avoid any bias.

3.2.1. Single Conditions Components

In single conditions, the BLP connectivity was almost completely described by the first BLP-PC, which explained 95% and 93.3% of the total variance, at rest and task, respectively. This component mainly loaded on alpha and beta bands in both conditions (Fig. 4).This is consistent, at least for rest, with the literature (e.g. (Brookes et al., 2011b, 2011a; de Pasquale et al., 2010), and our previous univariate analysis.

For BOLD connectivity, we identified 2 components both at rest and task, the first of which explains 68% (rest) and 76% (task) of the total variance, and it is a clear representation of the average BOLD-FC across subjects. While BOLD-PC1 reflects the segregation of RSN, with stronger within- than between-network correlation, BOLD-PC2 reflects the enhanced integration between VIS-DAN, and stronger communication within VIS, which is stronger during the visuospatial attention task (see Fig. 4).

The spatial topography of BOLD and BLP components was similar at rest and during tasks consistently with the previous analysis. Specifically, there was a significant correlation between BOLD-PC1 at rest and task (corr = 0.95, p < 10^{-7}, Mantel's test), and between BLP-PC1 at rest and task (corr = 0.93, p < 10^{-7}, Mantel's test), suggesting that the PC1 accounts for spatial patterns that do not modulate during the attentional task. In addition, we found that BLP-PC1 was significantly correlated with BOLD-PC1 both at rest and during task (rest: corr= 0.40, p = 0.016; task: corr = 0.42, p = 0.0011; all Bonferroni corrected) (Figure 4 middle panel, scatter plot). BLP-PC1 loaded on all bands, especially alpha and beta bands (Fig. 4 right). However, the similarity between BOLD- and BLP-PC1 do not reflect task-related changes, but only stronger within-than between-network interactions that are present both during rest and task conditions.

In summary, these findings show that both BOLD and BLP connectivity patterns are spatially low dimensional, and in the case of the BLP
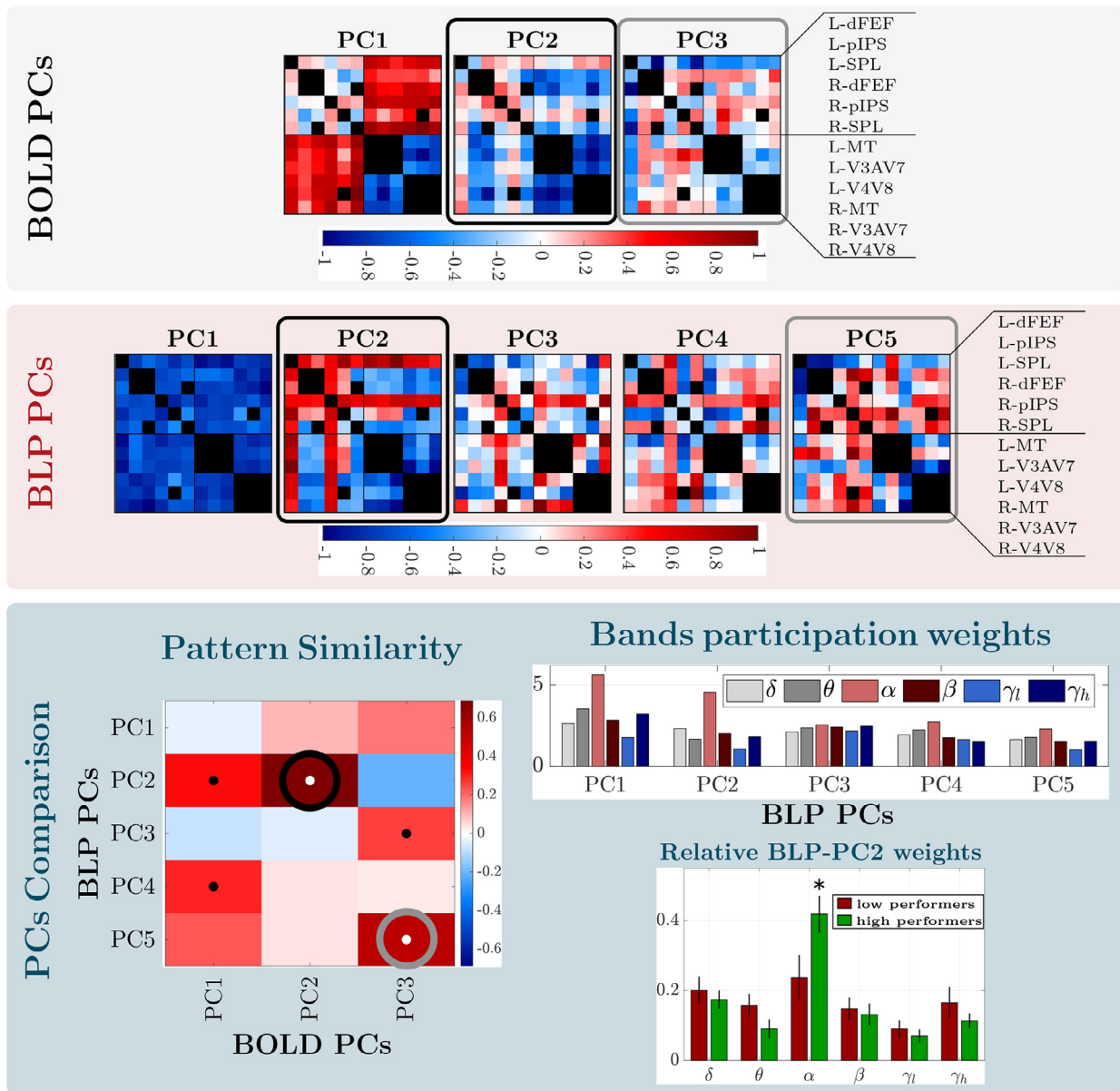
Fig. 5. Comparison between multi-band BLP- and BOLD- task–rest Principal Components. Top) BOLD Principal Components, sorted concerning the explained variance. PCs significantly similar ($p < 0.05$, Bonferroni corrected) to multi-band BLP-PCs are embedded in black and gray contours. Middle) Multi-band PCs sorted concerning the explained variance. BLP-PCs with a pattern significantly similar to the BOLD-PCs are embedded in black and gray contours. Bottom-left) Pattern similarity between each pair of BLP-PCs and BOLD-PCs. Colors represent the strength of the correlation, while white filled dots indicate values that are significantly different from zero (Mantel's Test, $p < 0.05$, Bonferroni corrected) and black dots mark significant, uncorrected comparisons. Bottom-right) Upper: Participation weights of each frequency band. These values represent the sum of the absolute weight values across subjects. Lower: Participation weights of each frequency band for the groups of subjects with low and high accuracy, together with statistical results (the average alpha weight of subjects with high accuracy is larger than all the other bands in both groups, * stands for $p < 0.0008$).

involve mainly alpha and beta bands. These patterns are similar between rest and task and correlate between modalities. Given the presence of such strong correlated spatial components across multiple frequency bands is not surprising that task–rest signals do not correlate between BOLD- and BLP-FC, especially for single frequencies (Fig. 3 bottom). This led us to examine multi-band relationships between BOLD and BLP connectivity.

3.2.2. Task–Rest Components

When the difference between task and rest is considered, the elbow method selected 3 PCs for fMRI and 5 PCs for BLP (see Fig. 5, for PC patterns; Figure S2, scree plots of all separations). Results of control analyses to test the robustness of the obtained separation are reported in *Supplementary Material* (*Section S2.4*).

The first BOLD-PC (42% of the total variance) is composed of an increase of DAN-VIS interactions along with a parallel decrease of interactions between the visual regions. BOLD-PC2 (15% of variance) shows increased connectivity between the left FEF, the right SPL, and, to a smaller extent, the right FEF regions (the latter at a smaller extent) with every other region, in parallel with decreased connectivity within the visual network. BOLD-PC3 (7% of variance) describes a general increase for all DAN-VIS connectivity pairs, except left FEF, and a weak FC decrement in the visual regions.

The first BLP-PC, which accounts for 43.78% of the total variance, reflects the non-spatially specific modulation, common to every frequency band, consistent with the global signal.

The BLP multi-band patterns were compared to the BOLD-PC through Pearson's correlation coefficient, whose significance was evaluated by a Mantel's Test with 15,000 permutations. The polarity of the BLP-PCs was set to produce, for each row in the similarity matrix (BLP-PC), a positive maximum correlation with the BOLD-PCs (see Fig. 5, bottom left).

The strongest pattern similarity (correlation = 0.69, p < 10^{-4}, Bonferroni corrected) occurs between BOLD-PC2 and BLP-PC2 (12.29% variance) and captures the increased interaction of the left FEF and right FEF-SPL (the latter at a lower extent) with other nodes of the DAN and VIS networks, as well as the decrements of connectivity in the VIS system. The weights of BLP-PC2 loads mainly on the alpha band, as confirmed by the main effect band (p < 0.00001) in the multivariate ANOVA and significant post-hoc tests (p < 0.0004). After splitting subjects into low and high performers based on the mean target discrimination accuracy, a significant interaction band x performance (p < 0.003) showed that alpha weights were significantly larger in high performers as compared to all other bands, as well as alpha weights in low performers (p < 0.0008, Fig. 5 bottom right).

The second strongest pattern similarity regards BOLD-PC3 and BLP-PC5 (correlation = 0.52, p = 0.003, Bonferroni corrected), with a similar distribution of weights across bands.

In a supplementary analysis (see *Supplementary Material S2.3.1*), we also compared single- vs. multi-band BLP PCs to explain BOLD-PC decomposition using the Bayesian Information Criterion (BIC). In general, we found multi-band BLP components to be a better descriptor of task-related fMRI connectivity changes. Fig. 6 shows a summary of BOLD-PC to BLP-PC correspondence with their regional topography and relative weights of the connectivity. BLP-PC2 is the one related to the accuracy during the task for weights on the alpha band.

4. Discussion

The goal of this study was to identify the neurophysiological correlates of functional connectivity changes, measured with fMRI (BOLD-FC) as observers go from a rest state (visual fixation) to a specific task state involving the allocation and shifts of visuospatial attention (Spadone et al., 2015). We focused on the static temporal correlation of amplitude fluctuations of band-limited power (BLP-FC) measured with MEG, which is considered the most consistent electrophysiological correlate of BOLD RSNs. We asked if these task–rest modulations occur in specific frequency bands or involve joint participation of multiple bands.

At the group level, we found an overall decrease of BLP-FC across two bands (alpha and beta) and an increase in the gamma band (Fig. 3, top). When separately considering rest and task states, we found a significant correlation between the topography of the BOLD-FC and that of BLP-FC in the alpha and beta bands (Fig. 3, bottom). Instead, no significant topography correlation occurred for task–rest FC modulation in any of the bands. This negative result is probably due to the low dimensionality of the electrophysiological patterns observed at rest and task conditions, focusing on a single component, which loads mostly in alpha and beta bands, and that does not change much between rest and task conditions (Fig. 4). This dominant pattern accounts (i) for the larger within- than between-network connectivity, in common with the first BOLD-FC pattern, and (ii) for the common signal in MEG, spread across all frequency bands (even though mostly in alpha and beta). The subtraction operation between task and rest connectivity removes this common electrophysiological factor and allows for different and higher dimensional patterns to emerge that cannot be resolved with a single-band approach.

In accordance with that, we found a significant similarity between task–rest BOLD and multi-band BLP functional connectivity patterns after orthogonalization through a PCA procedure. Two main patterns
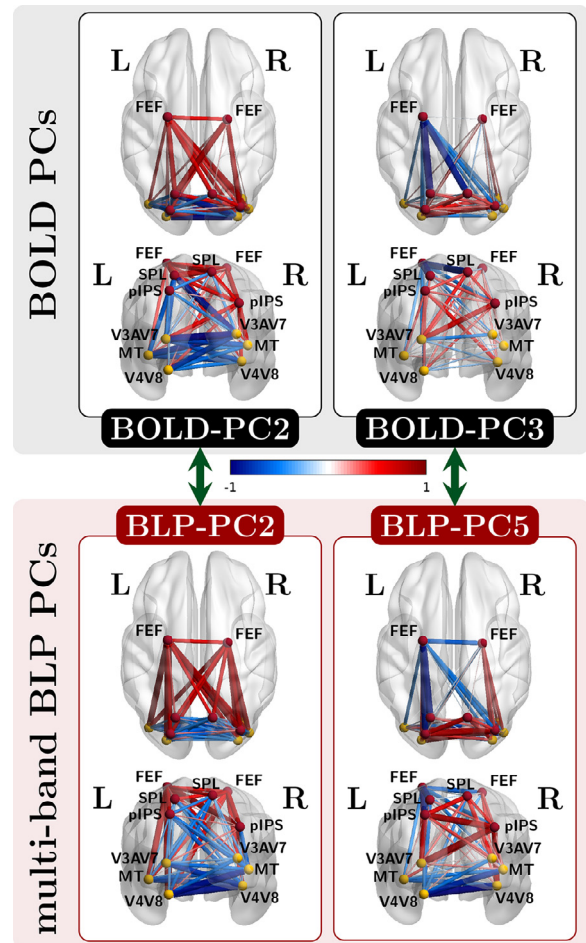

Fig. 6. Summary of the BOLD-BLP-PCs comparison. Spatial patterns of connectivity modulations representing the BLP-PCs corresponding to BOLD-PC2 and BOLD-PC3, all projected onto the MNI brain representation. Positive and negative values are coded in red and blue, respectively. Line thickness represents the strength of the modulation.

emerged: first, the interaction of left FEF and right SPL with other regions of the DAN and VIS along with a decrement of inter-regional VIS connectivity; second, the enhanced correlation between DAN and VIS regions. Notably, the alpha weight of the first pattern differed between subjects with low and high behavioral performance. These patterns resemble the main patterns identified in our previous fMRI study (Spadone et al., 2015), and correspond to a behaviorally relevant top-down influence from the DAN to the VIS network.

4.1. Association Between BLP-FC and BOLD-FC Task-Induced Modulations

Since the seminal work of Logothetis and colleagues in primates (Logothetis et al., 2001), BLP correlations have been proposed as the electrophysiological correlate of the resting-state networks (RSNs) measured through fMRI (Brookes et al., 2011b, 2011a; de Pasquale et al., 2010; de Pasquale et al., 2012; Hacker et al., 2017; He et al., 2008; Hipp et al., 2012; Keller et al., 2013; Leopold et al., 2003; Mantini et al., 2007). Most studies have emphasized that the similarity between BOLD RSNs and BLP RSNs is most reliable in the alpha and beta bands.

Our work is consistent with these observations. We find even at the level of single subjects a significant relationship between the magnitude of the BOLD and BLP correlation in alpha and beta bands, at rest, and during the attention task (Fig. 3).

However, even early studies showed that each fMRI RSNs is characterized by a specific electrophysiological signature that involves mul-

tiple brain rhythms (de Pasquale et al., 2010; Hipp et al., 2012; Mantini et al., 2007). Moreover, alpha and beta rhythms have the highest signal-to-noise (SNR) in the MEG signal, which may explain their more consistent relationship to fMRI RSNs. When SNR differences across bands are corrected, then BLP correlates of fMRI RSNs extends from delta to gamma band (Hipp and Siegel, 2015) (see also (Garcés et al., 2016)). Accordingly, we found multi-band BLP modulations when going from rest to attention. Two principal modulations occurred: first, an overall not-spatially-specific modulation of correlation across several bands, and second, coupled modulations of BLP across different rhythms corresponding to specific spatial patterns of BOLD-FC modulations.

The overall change of BLP correlation across nodes and networks reflects the modulated amplitude of the global signal that underlies increased vigilance during the attention task (Liu et al., 2018; Tal et al., 2013; Wong et al., 2013). This effect is quite strong, accounting for more than 40% of the variability across subjects, nodes, and bands. While there are different strategies to remove the global signal from fMRI data (Murphy and Fox, 2017), a whole-brain signal regression on BLP data is particularly challenging due to the difficulty to account for possible band-specific differences in the spectral contribution to the global signal. However, the multi-band PCA approach effectively isolates components representing modulation of the global signal from rest to task: although the participation weight of the alpha band to the BLP-PC1 provides the largest contribution to this overall modulation, the weights of the other bands are not negligible (Fig. 5). Thus, multi-band BLP-PC1 might reflect a broadband electrophysiological signal related to the BOLD ongoing global signal (Wen and Liu, 2016), which was instead removed from fMRI data before estimating the FC. Changes in MEG global signal as a function of task conditions is still a relatively unexplored topic worth future investigation given the robustness of this effect.

The second effect was a spatially specific multi-band modulation of BLP correlation involving nodes of the dorsal attention network (FEF, IPS, SPL) and nodes of the VIS network. There are three main elements to this interaction in the fMRI data: (1) an increase of correlation between left FEF and right SPL with all other nodes of the DAN and VIS; (2) a decrease of correlation within the VIS; (3) an increased correlation between DAN and VIS nodes (Fig. 4, 5, 6). These elements are captured by the BOLD PCA: PC1 captures (2)(3); BOLD PC2 captures (1)(2), and BOLD PC3 captures (3).

BOLD-PC2 (15% of the total variance) captures the increased interaction between left FEF and right FEF-SPL with other nodes of the DAN and VIS networks, as well as the decrements of connectivity in the VIS system. BOLD-PC2 shows the largest pattern similarity with BLP-PC2 loading mainly in the alpha band. The increased correlation between FEF and other regions shown in BOLD-PC2 and the corresponding BLP-PC2 is consistent with the known FEF role in establishing cue-related preparatory signals (Corbetta and Shulman, 2002) and exerting top-down influence on sensory processing (Bressler et al., 2008; Heinen et al., 2017; Moore, 1999), modulating activity and connectivity with the visual occipital cortex.

The weights of BLP-PC2, especially in the alpha band, were predictive of accuracy across subjects. This result is consistent with the previously observed positive relationship between accuracy and FEF-VIS connectivity changes during the attention task in Spadone et al. (Spadone et al., 2015). The link between alpha band BLP and performance is consistent with a large literature on alpha power modulation in attention paradigms. Modulation of alpha activity has traditionally been associated with inhibition of the not-to-be-attended side (Jensen et al., 2012) and anticipation of a visual target (Bonnefond and Jensen, 2012; Jensen et al., 2012; Sauseng et al., 2008; Thut et al., 2006). While these paradigms have reported attention-related modulation in the order of hundreds of milliseconds to seconds, time-locked to specific events (cue or target), our data indicate more sustained modulations of alpha band connectivity (tens of seconds) related to attention performance. Similar longer times scale behaviorally relevant modulations capturing individ-

ual variability have been reported in many fMRI connectivity studies (Rosenberg et al., 2020; Sestieri et al., 2013; Spadone et al., 2015).

The second association involved BOLD-PC3 (7% of variance) and BLP-PC5. BOLD-PC3 describes a general increase of all DAN-VIS connectivity pairs, except for left FEF, which was instead clearly involved in PC2. Previous studies have also shown broadband modulations in attention tasks (Siegel et al., 2008).

How do we account for these multi-band patterns of task–rest modulation?

On one hand, the higher SNR of the alpha band compared with the other bands (Hipp and Siegel, 2015) may be the reason why the modulation in other bands does not appear to be significantly associated with behavioral performance.

On the other hand, a second explanation is that the modulation of different frequencies carries different kinds of information. For instance, (Magri et al., 2012) found that fluctuations of the BOLD signal in the visual cortex co-varied with the power of alpha, beta, and gamma LFP bands. However, alpha/gamma relationships were informative about the amplitude of the BOLD signal, while beta/gamma informed the latency of BOLD.

In general, consistently with these results, we find that decreases in alpha/beta bands were associated with increases in high gamma (Figure 3). It is also consistent with electrophysiological evidence that LFP power <20 Hz is important for distant BOLD connectivity (Wang et al., 2012), and that low frequencies play a role in large-scale coordination (Bressler et al., 2008; Schroeder and Lakatos, 2009).

4.2. Methodological Considerations on the Spatial Separation of Common Patterns

Our choice of applying the Principal Components Analysis to seek for the electrophysiological correlates of the BOLD connectivity changes observed when going from fixation to a task condition was based on several considerations. (i) At first, we wanted to extract information from the data, taking into account the across-subjects variability observed in task–rest connectivity matrices. We observed that the coefficient of variation (CV) of task–rest connectivity values across subjects was significantly larger than chance, and different than single conditions (rest, task) in fMRI (see *Supplementary Material S2*.2). This observation indicates that the average task–rest BOLD FC matrix represents only part of the information contained in the data. (ii) Moreover, we wanted to select common (across subjects) spatial patterns of task-induced connectivity changes through a data-driven approach, where no initial assumptions are considered. This differentiates, for instance, from the application of the generalized linear model (GLM), a hypothesis-driven approach, where the set of regressors should be designed a-priori and validated by the results. In absence of any initial hypotheses, we thus preferred to implement a more flexible data-driven technique. (iii) Another important consideration regards the variables to be considered for BOLD-FC and BLP-FC comparison. Indeed, the PCA application is a suitable tool to reduce the number of variables to be compared by considering only the patterns by PCA rather than all the pairwise correlation values. Finally, (iv) with this spatial separation, we accounted for the high positive correlations observed in BLP-FC across regions and bands.

Notably, the first three motivations do not exclusively apply to BLP-FC data, but also BOLD-FC data. Importantly, spatial separation techniques have been already applied to BOLD-FC in recent studies exploiting the inter-subjects variability of connectivity through a relationship with behavioral measures (Amico and Goñi, 2018), or multimodal (EEG-fMRI) topological similarity (Wirsich et al., 2020), even though the common BOLD signal was removed as in our study. Notably, we also applied multivariate PCA to single-condition connectivity maps, which was used to extract connectivity patterns common across subjects. We indeed obtained a dominant pattern in the two conditions and modalities (PC1). Even though BOLD and BLP PC1 were correlated, this does not provide information about BOLD-BLP association during task-

related changes, and the single condition analysis explains why standard single-frequency cross-modality comparisons of task vs. rest correlation changes did not produce significant associations (Fig. 3).

The main limitation of PCA is the absence of suitable statistics to verify the results. This is the reason why we tested the robustness of the PCs through a leave-one-out test over subjects, described in the *Supplementary Material* (*Sections S1.5 and S2.4*).

5. Conclusions

We found that the spatial patterns of BOLD connectivity modulation observed when going from rest to a visuospatial attention task cannot be directly associated with single-band BLP modulations. Rather, BOLD components representing common patterns across subjects can be best recapitulated by multi-band components of MEG connectivity. Specifically, we found that cross-network increases between dorsal attention and visual networks, and the concomitant decreases within the visual network are associated with concordant modulations in all the bands, with a primary role of the alpha band.

Declaration of Competing Interest

None

Credit authorship contribution statement

Chiara Favaretto: Writing - original draft, Software, Formal analysis, Writing - review & editing. **Sara Spadone:** Data curation, Investigation. **Carlo Sestieri:** Investigation, Writing - review & editing. **Viviana Betti:** Writing - review & editing. **Angelo Cenedese:** Writing - review & editing. **Stefania Della Penna:** Conceptualization, Writing - review & editing, Supervision. **Maurizio Corbetta:** Conceptualization, Writing - review & editing, Supervision .

Acknowledgements

Supplementary materials

Supplementary material associated with this article can be found, in the online version, at doi:10.1016/j.neuroimage.2021.117781.

References

Amico, E., Goñi, J., 2018. The quest for identifiability in human functional connectomes. Sci. Rep. 8, 8254. doi:10.1038/s41598-018-25089-1.

Betti, V., Corbetta, M., de Pasquale, F., Wens, V., Della Penna, S., 2018. Topology of functional connectivity and hub dynamics in the beta band as temporal prior for natural vision in the human brain. J. Neurosci. 1017–1089. doi:10.1523/JNEUROSCI.1089-17.2018.

Betti, V., Della Penna, S., de Pasquale, F., Mantini, D., Marzetti, L., Romani, G.L., Corbetta, M., Penna, S., Della, Pasquale, F., De, Mantini, D., Marzetti, L., Romani, G.L., DellaPenna, S., de Pasquale, F., Mantini, D., Marzetti, L., Romani, G.L., Corbetta, M., Della Penna, S., de Pasquale, F., Mantini, D., Marzetti, L., Romani, G.L., Corbetta, M., 2013. Natural scenes viewing alters the dynamics of functional connectivity in the human brain. Neuron 79, 782–797. doi:10.1016/j.neuron.2013.06.022.

Bonnefond, M., Jensen, O., 2012. Alpha oscillations serve to protect working memory maintenance against anticipated distracters. Curr. Biol. 22, 1969–1974. doi:10.1016/j.cub.2012.08.029.

Brainard, D.H., 1997. The psychophysics toolbox. Spat. Vis. 10, 433–436. doi:10.1163/156856897X00357.

Bressler, S.L., Tang, W., Sylvester, C.M., Shulman, G.L., Corbetta, M., 2008. Top-down control of human visual cortex by frontal and parietal cortex in anticipatory visual spatial attention. J. Neurosci. 28, 10056–10061. doi:10.1523/JNEUROSCI.1776-08.2008.

Brookes, M.J., Hale, J.R., Zumer, J.M., Stevenson, C.M., Francis, S.T., Barnes, G.R., Owen, J.P., Morris, P.G., Nagarajan, S.S., 2011a. Measuring functional connectivity using MEG: Methodology and comparison with fcMRI. Neuroimage 56, 1082–1104. doi:10.1016/j.neuroimage.2011.02.054.

Brookes, M.J., Woolrich, M., Luckhoo, H., Price, D., Hale, J.R., Stephenson, M.C., Barnes, G.R., Smith, S.M., Morris, P.G., 2011b. Investigating the electrophysiological basis of resting state networks using magnetoencephalography. Proc. Natl. Acad. Sci. 108, 16783–16788. doi:10.1073/pnas.1112685108.

Capotosto, P., Spadone, S., Tosoni, A., Sestieri, C., Romani, G.L., Della Penna, S., Corbetta, M., 2015. Dynamics of EEG rhythms support distinct visual selection mechanisms in parietal cortex: a simultaneous transcranial magnetic stimulation and EEG study. J. Neurosci. 35, 721–730. doi:10.1523/JNEUROSCI.2066-14.2015.

Capotosto, P., Tosoni, A., Spadone, S., Sestieri, C., Perrucci, M.G., Romani, G.L., Della Penna, S., Corbetta, M., 2013. Anatomical segregation of visual selection mechanisms in human parietal cortex. J. Neurosci. 33, 6225–6229. doi:10.1523/JNEUROSCI.4983-12.2013.

Cattell, R.B., 1966. The Scree test for the number of factors. Multivariate Behav. Res. 1, 245–276. doi:10.1207/s15327906mbr0102_10.

Cole, M.W., Bassett, D.S., Power, J.D., Braver, T.S., Petersen, S.E., 2014. Intrinsic and task-evoked network architecture of the human brain. Neuron 83, 238–251. doi:10.1016/j.neuron.2014.05.014.

Corbetta, M., Shulman, G.L., 2002. Control of goal-directed and stimulus-driven attention in the brain. Nat. Rev. Neurosci. 3, 201–215. doi:10.1038/nrn755.

others de Pasquale, F., Della Penna, S., Snyder, A.Z., Lewis, C., Mantini, D., Marzetti, L., Belardinelli, P., Ciancetta, L., Pizzella, V., Romani, G.L., Corbetta, M., 2010. Temporal dynamics of spontaneous MEG activity in brain networks. Proc. Natl. Acad. Sci. 107, 200913863. doi:10.1073/pnas.0913863107.

de Pasquale, F., Della Penna, S., Snyder, A.Z., Marzetti, L., Pizzella, V., Romani, G.L., Corbetta, M., De Pasquale, F., Della Penna, S., Snyder, A.Z., Marzetti, L., Pizzella, V., Romani, G.L., Corbetta, M., 2012. A cortical core for dynamic integration of functional networks in the resting human brain. Neuron 74, 753–764. doi:10.1016/j.neuron.2012.03.031.

Della Penna, S., Corbetta, M., Wens, V., de Pasquale, F., 2019. The Impact of the Geometric Correction Scheme on MEG Functional Topology at Rest. Front. Neurosci. 13, 1–19. doi:10.3389/fnins.2019.01114.

Della Penna, S., Delgratta, C., Granata, C., Pasquarelli, A., Pizzella, V., Rossi, R., Russo, M., Torquatiand, K., Erné, S.N., Del Gratta, C., Granata, C., Pasquarelli, A., Pizzella, V., Rossi, R., Russo, M., Torquati, K., Erné, S.N., 2000. Biomagnetic systems for clinical use. Philos. Mag. B 80, 937–948. doi:10.1080/01418630008221960.

Della Penna, S., Torquati, K., Pizzella, V., Babiloni, C., Franciotti, R., Rossini, P.M., Romani, G.L., 2004. Temporal dynamics of alpha and beta rhythms in human SI and SII after galvanic median nerve stimulation. A MEG study. Neuroimage 22 (4), 1438–1446. doi:10.1016/j.neuroimage.2004.03.045.

Forman, S.D., Cohen, J.D., Fitzgerald, M., Eddy, W.F., Mintun, M.A., Noll, D.C., 1995. Improved assessment of significant activation in functional magnetic resonance imaging (fMRI): use of a cluster-size threshold. Magn. Reson. Med. 33, 636–647. doi:10.1002/mrm.1910330508.

Garcés, P., Pereda, E., Hernández-Tamames, J.A., Del-Pozo, F., Maestú, F., Ángel Pineda-Pardo, J., 2016. Multimodal description of whole brain connectivity: a comparison of resting state MEG, fMRI, and DWI: Multimodal description of whole brain connectivity. Hum. Brain Mapp. 37, 20–34. doi:10.1002/hbm.22995.

Hacker, C.~D.C.D., Snyder, A.Z.A.~Z., Pahwa, M., Corbetta, M., Leuthardt, E.C.E.~C., Leuthardt, C., 2017. Frequency-specific electrophysiologic correlates of resting state fMRI networks. Neuroimage 149, 446–457. doi:10.1016/j.neuroimage.2017.01.054.

He, B.J., Snyder, A.Z., Zempel, J.M., Smyth, M.D., Raichle, M.E., 2008. Electrophysiological correlates of the brain's intrinsic large-scale functional architecture. Proc. Natl. Acad. Sci 105, 16039–16044. doi:10.1073/pnas.0807010105.

Heinen, K., Feredoes, E., Ruff, C.C., Driver, J., 2017. Functional connectivity between prefrontal and parietal cortex drives visuo-spatial attention shifts. Neuropsychologia 99, 81–91. doi:10.1016/j.neuropsychologia.2017.02.024.

Hipp, J.F., Hawellek, D.J., Corbetta, M., Siegel, M., Engel, A.K., 2012. Large-scale cortical correlation structure of spontaneous oscillatory activity. Nat. Neurosci. 15, 884. doi:10.1038/nn.3101.

Hipp, J.F., Siegel, M., 2015. BOLD fMRI correlation reflects frequency-specific neuronal correlation. Curr. Biol. 25, 1368–1374. doi:10.1016/j.cub.2015.03.049.

Jensen, O., Bonnefond, M., VanRullen, R., 2012. An oscillatory mechanism for prioritizing salient unattended stimuli. Trends Cogn. Sci. doi:10.1016/j.tics.2012.03.002.

Keller, C.J., Bickel, S., Honey, C.J., Groppe, D.M., Entz, L., Craddock, R.C., Lado, F.A., Kelly, C., Milham, M., Mehta, A.D., 2013. Neurophysiological investigation of spontaneous correlated and anticorrelated fluctuations of the BOLD signal. J. Neurosci. 33, 6333–6342. doi:10.1523/JNEUROSCI.4837-12.2013.

Kleiner, M., Brainard, D., Pelli, D., Ingling, A., Murray, R., Broussard, C., 2007. What's new in Psychtoolbox-3. Perception 36 (14), 1.

Larson-prior, L.J., Oostenveld, R., Penna, Della, Stefania, Michalareas, G., Prior, F., Babajani-feremi, A., Schoffelen, J.-M., Marzetti, L., de Pasquale, Francesco, Di Pompeo, F., others, Penna, S Della, Michalareas, G., Prior, F., Babajani-feremi, A., Schoffelen, J.-M., Marzetti, L., Pasquale, F De, Pompeo, F.Di, Stout, J., Woolrich, M., Luo, Q., Bucholz, R., Fries, P., Pizzella, V., Romani, G.L., Corbetta, M., Snyder, A.Z., Hcp, W., 2013. Adding dynamics to the Human Connectome Project with MEG. Neuroimage 80, 190–201. doi:10.1016/j.neuroimage.2013.05.056.

Lattin, J.M., Carroll, J.D., Green, P.E., 2003. Analyzing multivariate data. Analyzing multivariate data. Thomson Brooks/Cole, Pacific Grove, CA.

Leopold, D.A., Murayama, Y., Logothetis, N.K., 2003. Very slow activity fluctuations in monkey visual cortex: implications for functional brain imaging. Cereb. cortex 13, 422–433. doi:10.1093/cercor/13.4.422.

Liljeström, M., Stevenson, C., Kujala, J., Salmelin, R., 2015. Task- and stimulus-related cortical networks in language production: exploring similarity of MEG- and fMRI-derived functional connectivity. Neuroimage 120, 75–87. doi:10.1016/j.neuroimage.2015.07.017.

Liu, T.T., Nalci, A., Falahpour, M., Jolla, L., Drive, G., Jolla, L., 2018. The Global Signal in fMRI: Nuisance or Information? Neuroimage 213–229. doi:10.1016/j.neuroimage.2017.02.036.

Liu, Z., Fukunaga, M., de Zwart, J.A., Duyn, J.H., 2010. Large-scale spontaneous fluctuations and correlations in brain electrical activity observed with magnetoencephalography. Neuroimage 51, 102–111. doi:10.1016/j.neuroimage.2010.01.092.

Logothetis, N.K., Pauls, J., Augath, M., Trinath, T., Oeltermann, A., 2001. Neurophysiological investigation of the basis of the fMRI signal. Nature 412, 150. doi:10.1038/35084005.

Magri, C., Schridde, U., Murayama, Y., Panzeri, S., Logothetis, N.K., 2012. The amplitude and timing of the BOLD signal reflects the relationship between local field potential power at different frequencies. J. Neurosci. 32, 1396–1407. doi:10.1523/JNEUROSCI.3985-11.2012.

Mantel, N., Haenszel, W., 1959. Statistical aspects of the analysis of data from retrospective studies of disease. J. Natl. cancer Inst. 22, 719–748. doi:10.1093/jnci/22.4.719.

Mantini, D., Penna, S.Della, Marzetti, L., De Pasquale, F., Pizzella, V., Corbetta, M., Romani, G.L., 2011. A signal-processing pipeline for magnetoencephalography resting-state networks. Brain Connect 1, 49–59. doi:10.1089/brain.2011.0001.

Mantini, D., Perrucci, M.G., Del Gratta, C., Romani, G.L., Corbetta, M., 2007. Electrophysiological signatures of resting state networks in the human brain. Proc. Natl. Acad. Sci 104, 13170–13175. doi:10.1073/pnas.0700668104.

Moore, T., 1999. Shape representations and visual guidance of saccadic eye movements. Science 285 (80–.), 1914–1917. doi:10.1126/science.285.5435.1914.

Murphy, K., Fox, M.D., 2017. Towards a consensus regarding global signal regression for resting state functional connectivity MRI. Neuroimage 154, 169–173. doi:10.1016/j.neuroimage.2016.11.052.

Pelli, D.G., 1997. The VideoToolbox software for visual psychophysics: Transforming numbers into movies. Spat. Vis. 10, 437–442. doi:10.1163/156856897X00366.

Pizzella, V., Della Penna, S., Del Gratta, C., Romani, G.L., 2001. SQUID systems for biomagnetic imaging. Supercond. Sci. Technol. 14, R79. doi:10.1088/0953-2048/14/7/201.

Rosenberg, M.D., Scheinost, D., Greene, A.S., Avery, E.W., Kwon, Y.H., Finn, E.S., Ramani, R., Qiu, M., Todd Constable, R., Chun, M.M., 2020. Functional connectivity predicts changes in attention observed across minutes, days, and months. Proc. Natl. Acad. Sci. U. S. A. 117, 3797–3807. doi:10.1073/pnas.1912226117.

Sauseng, P., Klimesch, W., Gruber, W.R., Birbaumer, N., 2008. Cross-frequency phase synchronization: A brain mechanism of memory matching and attention. Neuroimage 40, 308–317. doi:10.1016/j.neuroimage.2007.11.032.

Schroeder, C.E., Lakatos, P., 2009. Low-frequency neuronal oscillations as instruments of sensory selection. Trends Neurosci 32, 9–18. doi:10.1016/j.tins.2008.09.012.

Sebastiani, V., de Pasquale, F., Costantini, M., Mantini, D., Pizzella, V., Romani, G.L., Della Penna, S., 2014. Being an agent or an observer: different spectral dynamics revealed by MEG. Neuroimage 102, 717–728. doi:10.1016/j.neuroimage.2014.08.031.

Sestieri, C., Corbetta, M., Spadone, S., Romani, G.L., Shulman, G.L., 2013. Domain-general signals in the cingulo-opercular network for visuospatial attention and Episodic Memory. J. Cogn. Neurosci. 26, 551–568. doi:10.1162/jocn_a_00504.

Shulman, G.L., Astafiev, S.V, Franke, D., Pope, D.L.W., Snyder, A.Z., McAvoy, M.P., Corbetta, M., 2009. Interaction of stimulus-driven reorienting and expectation in ventral and dorsal frontoparietal and basal ganglia-cortical networks. J. Neurosci. 29, 4392–4407. doi:10.1523/JNEUROSCI.5609-08.2009.

Shulman, G.L., Pope, D.L.W., Astafiev, S.V, McAvoy, M.P., Snyder, A.Z., Corbetta, M., 2010. Right hemisphere dominance during spatial selective attention and target detection occurs outside the dorsal Frontoparietal Network. J. Neurosci. 30, 3640–3651. doi:10.1523/JNEUROSCI.4085-09.2010.

Siegel, M., Donner, T.H., Oostenveld, R., Fries, P., Engel, A.K., 2008. Neuronal synchronization along the dorsal visual pathway reflects the focus of spatial attention. Neuron 60, 709–719. doi:10.1016/j.neuron.2008.09.010.

Smith, S.M., Fox, P.T., Miller, K.L., Glahn, D.C., Fox, P.M., Mackay, C.E., Filippini, N., Watkins, K.E., Toro, R., Laird, A.R., Beckmann, C.F., 2009. Correspondence of the brain's functional architecture during activation and rest. Proc. Natl. Acad. Sci. 106, 13040–13045. doi:10.1073/pnas.0905267106.

Spadone, S., de Pasquale, F., Mantini, D., Della Penna, S., 2012. A K-means multivariate approach for clustering independent components from magnetoencephalographic data. Neuroimage 62, 1912–1923. doi:10.1016/j.neuroimage.2012.05.051.

Spadone, S., Della Penna, S., Sestieri, C., Betti, V., Tosoni, A., Perrucci, M.G., Romani, G.L., Corbetta, M., 2015. Dynamic reorganization of human resting-state networks during visuospatial attention. Proc. Natl. Acad. Sci. 112, 8112–8117. doi:10.1073/pnas.1415439112.

Tal, O., Diwakar, M., Wong, C.W., Olafsson, V., Lee, R., Huang, M.X., Liu, T.T., 2013. Caffeine-induced global reductions in resting-state BOLD connectivity reflect widespread decreases in MEG connectivity. Front. Hum. Neurosci. 7, 1–10. doi:10.3389/fnhum.2013.00063.

Tavor, I., Parker Jones, O., Mars, R.B., Smith, S.M., Behrens, T.E., Jbabdi, S., 2016. Task-free MRI predicts individual differences in brain activity during task performance. Science (80-.) 352, 216–220. doi:10.1126/science.aad8127.

Thut, G., Nietzel, A., Brandt, S.A., Pascual-Leone, A., 2006. α-Band electroencephalographic activity over occipital cortex indexes visuospatial attention bias and predicts visual target detection. J. Neurosci. 26, 9494–9502. doi:10.1523/JNEUROSCI.0875-06.2006.

Wang, liang, Saalmann, Y.B., Pinsk, M.A., Arcaro, M.J., Kastner, S., 2012. frequency coupling contributes to BOLD connectivity. Neuron 76, 1010–1020. doi:10.1016/j.neuron.2012.09.033.Electrophysiological.

Wen, H., Liu, Z., 2016. Broadband electrophysiological dynamics contribute to global resting-state fMRI signal. J. Neurosci. 36, 6030–6040. doi:10.1523/JNEUROSCI.0187-16.2016.

Wens, V., Marty, B., Mary, A., Bourguignon, M., Op De Beeck, M., Goldman, S., Van Bogaert, P., Peigneux, P., De Tiège, X., 2015. A geometric correction scheme for spatial leakage effects in MEG/EEG seed-based functional connectivity mapping. Hum. Brain Mapp. 36, 4604–4621. doi:10.1002/hbm.22943.

Wirsich, J., Amico, E., Giraud, A.-L., Goñi, J., Sadaghiani, S., 2020. Multi-timescale hybrid components of the functional brain connectome: a bimodal EEG-fMRI decomposition. Netw. Neurosci. 4, 658–677. doi:10.1162/netn_a_00135.

Wong, C.W., Olafsson, V., Tal, O., Liu, T.T., 2013. The amplitude of the resting-state fMRI global signal is related to EEG vigilance measures. Neuroimage 83, 983–990. doi:10.1016/j.neuroimage.2013.07.057.